Nanoscale

PAPER

View Article Online
View Journal | View Issue

Check for updates

Cite this: *Nanoscale*, 2018, **10**, 8712

High-temperature superconductivity at the lanthanum cuprate/lanthanum–strontium nickelate interface†

F. Baiutti,* G. Gregori, Y. E. Suyolcu, Y. Wang, G. Cristiani, W. Sigle, P. A. van Aken, G. Logvenov and J. Maier

Received 31st January 2018,
Accepted 12th March 2018

DOI: 10.1039/c8nr00885j

rsc.li/nanoscale

The utilization of interface effects in epitaxial systems at the nanoscale has emerged as a very powerful approach for engineering functional properties of oxides. Here we present a novel structure fabricated by a state-of-the-art oxide molecular beam epitaxy method and consisting of lanthanum cuprate and strontium (Sr)-doped lanthanum nickelate, in which interfacial high-temperature superconductivity (T_c up to 40 K) occurs at the contact between the two phases. In such a system, we are able to tune the superconducting properties simply by changing the structural parameters. By employing electron spectroscopy and microscopy combined with dedicated conductivity measurements, we show that decoupling occurs between the electronic charge carrier and the cation (Sr) concentration profiles at the interface and that a hole accumulation layer forms, which dictates the resulting superconducting properties. Such effects are rationalized in the light of a generalized space-charge theory for oxide systems that takes account of both ionic and electronic redistribution effects.

Open Access Article. Published on 14 March 2018. Downloaded on 1/13/2026 12:12:27 PM.
This article is licensed under a Creative Commons Attribution 3.0 Unported Licence.

1. Introduction

In recent years, the investigation of interface effects in oxide structures has led to unprecedented improvements of materials' properties and even to the occurrence of unexpected functionalities. Such a vibrant field provides disruptive opportunities for the development of next-generation nanoscaled devices.[1] The approach of oxide material engineering through the deliberate utilization of interfacial properties has seen early development in the field of ionic and mixed ionic-electronic conductors,[2,3] which nowadays crucially shape the development of devices for energy storage and conversion.[4] Here, massive deviations of the concentration of mobile ionic and electronic species may occur at material discontinuities (*e.g.* grain boundaries and dislocations) compared to the bulk (*i.e.* discontinuity-free) situation, leading in some cases to huge changes in the overall functionalities of the system under consideration.[5–8] It has been shown that such situations can be largely explained in the light of the space-charge theory.[9,10] More recently, an analogous approach has been implemented in thin film heterostructures (possessing a well-controlled geometry and superior quality), which allowed for the epitaxial coupling of a vast array of materials. This concept has yielded the occurrence of unexpected interface properties including interface electrical conductivity,[11,12] magnetism,[13,14] superconductivity[15,16] and high-temperature superconductivity.[17–19] Such effects, which are typically confined within a few nanometers across an interface and which do not belong to the single constituting phases, have been ascribed to different phenomena comprising *inter alia* epitaxial strain,[20,21] electronic charge transfer[22] and cationic and anionic local non-stoichiometry.[23–26]

In this context, we present here a comprehensive study of the structural and functional properties of heterostructures composed of lanthanum cuprate (La_2CuO_4–LCO) and Sr-doped lanthanum nickelate ($La_{2-x}Sr_xNiO_4$–LSNO), fabricated by atomic-layer-by-layer molecular beam epitaxy (ALL-MBE),[27] and we demonstrate that high-temperature superconductivity (superconducting critical temperature T_c up to ≈40 K) can be induced in LCO at the contact with LSNO, even though neither of the two phases alone exhibit superconductivity *per se*.

While it is well known that LCO undergoes an insulator-to-high-temperature-superconductor transition upon hole ($h^{\bullet}$) doping (this is normally achieved, in the bulk form, by introducing interstitial oxygen or acceptor dopants – zero-dimensional or homogeneous doping),[28,29] recent experiments dealt with the occurrence of local high-temperature superconductivity (HTSC) in LCO as a consequence of interface effects (two-dimensional or heterogeneous doping).[19] However, so far, this

Max Planck Institute for Solid State Research, Heisenbergstr. 1, 70569 Stuttgart, Germany. E-mail: fbaiutti@irec.cat

†Electronic supplementary information (ESI) available. See DOI: 10.1039/c8nr00885j

This journal is © The Royal Society of Chemistry 2018

Open Access Article. Published on 14 March 2018. Downloaded on 1/13/2026 12:12:27 PM. This article is licensed under a Creative Commons Attribution 3.0 Unported Licence.

has been limited to homoepitaxial systems in which the only employed phase was LCO-based (*e.g.* interfacial HTSC in Sr-doped LCO/LCO bilayers and superlattices or in two-dimensionally doped LCO):[17,19,30,31] Here instead it is shown, for the first time, that interface HTSC can be induced in LCO also at the heteroepitaxial contact with LSNO. Furthermore, we demonstrate that the final superconducting properties of the LCO/LSNO interface can be effectively tuned by simply changing the structural parameters (doping level x of the nickelate phase, layers sequencing and spacing) while leaving the stoichiometry of LCO unchanged, unlike the "classical" bulk-doping picture. Finally, superconductivity is rationalized by considering a mechanism for hole accumulation at the interface based on local cationic intermixing but also on space-charge considerations.

The present work demonstrates the power of heterogeneous doping for local HTSC by introducing a novel successful example related to heteroepitaxial systems and proposes a comprehensive thermodynamic picture for oxide interfaces.

2. Results

La_2CuO_4 and La_2NiO_4 share the same Ruddlesden–Popper structure ($AO(ABO_3)_n$, A = La, B = Cu, Ni, n = 2) and can be addressed by similar chemical and defect-chemical considerations. Starting from the insulating stoichiometric compounds, an electronic phase transformation can be achieved by increasing the electron hole concentration $p = [h^{\bullet}]$. In particular, in the case of LNO a transition into a metallic phase with increasing p (up to $p \approx 1.0$) is observed,[32] whereas high-temperature superconductivity (for $0.05 \leq p \leq 0.36$) and metallicity ($p > 0.36$) appear in LCO.[33] A hole increase can be generated in LCO and LNO by substituting La with an acceptor dopant (mostly Sr^{2+}, denoted by Sr'_{La} *i.e.* Sr on the La-site with negative excess charge) or by intercalating oxygen excess in the form of interstitial defects (O''_i) (homogeneous doping).[34–37] Taking into account that both $La_{2-x}Sr_xCuO_4$ (LSCO) and LSNO can also accommodate a large amount of double-positively charged oxygen vacancies ($V_O^{\bullet\bullet}$), the electroneutrality condition reads:

$$p + 2[V_O^{\bullet\bullet}] = 2[O''_i] + [Sr'_{La}] \quad (1)$$

The coupling between the various defect concentrations is determined by the mass action laws of the respective interaction reactions (Frenkel-disorder reaction and oxygen incorporation reaction).[34] At interfaces eqn (1) has to be replaced by Poisson's equation. A chemical potential gradient for holes and oxygen vacancies, as well as for Sr, is present once a contact between nominally undoped LCO and LSNO is formed. In order to establish equilibrium conditions, an interdiffusion of all the mobile defect species between LSNO and LCO should take place,[38,39] which in turn is expected to deeply affect the final conduction properties of the interface region.

In order to investigate such a situation, superlattices have been realized by the atomic-layer-by layer oxide MBE technique, which allows for a precise control of the film stoichiometry at the atomic layer level. The nominal composition of the superlattices can be written as:

$$1\times La_{1.56}Sr_{0.44}CuO_4 + S \times (2.5 \times La_{2-x}Sr_xNiO_4 + N \times La_2CuO_4) \quad (2)$$

(see ESI Fig. S1 and S2† for *in situ* and *ex situ* structural characterization and ref. 27 for details on the growth method). Here S represents the number of superlattice unit repetitions, whereas N defines the thickness of the LCO phase (expressed in number of unit cells – u.c.).

The resistance data for a representative set of samples having different doping levels x of LSNO are shown in Fig. 1 (panel a). Remarkably, for increasing x, high-temperature superconductivity appears. In Fig. 1b, the T_c values as a function of the doping level are summarized. Superconductivity is found for $x > 0.5$, reaching the plateau value of ≈35–40 K for $x > 0.8$. It is important to note here that none of the constituting materials, with the stoichiometry as expressed by eqn (2), is expected to exhibit superconductivity. Rather, high-temperature superconductivity is induced in the LCO phase at the interface region as a consequence of the contact with the nickelate phase. (Please consider that, after the growth, the system has been equilibrated under vacuum conditions, so that the presence of oxygen interstitials in the bulk, which could in principle have a role in the occurrence of HTSC in LCO, can be ruled out – see the Experimental section and ref. 40). As far as the temperature dependence of the resistance is concerned ($\partial R/\partial T$), one cannot infer a clear correlation with the doping level x of LSNO. This, together with a certain broadness which characterizes the superconducting transition (see ESI Table S1† for the data on the superconducting transition and for the definition of T_c), is suggestive of spatial inhomogeneities in the charge distribution or to a certain crystallographic disorder at the interface (this is especially true for high x values due to the abundance of oxygen vacancies in LSNO).

In Fig. 1c and d, the electrical behavior of bilayers having different contents x for LSNO is reported. Such structures, in which LCO is either deposited as a bottom or as a top layer for LSNO, allows for addressing the electrical properties of single contacts between the phases. In particular, in Fig. 1c (d), the R *vs.* T curve for a structure in which LCO is a bottom (top) layer is displayed. Notably, by comparing the two, one can notice that the superconducting properties are only slightly affected by the layer sequence, *i.e.* the maximum T_c is, in both cases, ≈24 K. Moreover, the analysis of the dependence of T_c on x suggests that the minimum doping level for the occurrence of HTSC is slightly higher in the case of the LCO (bottom layer)/LSNO (top layer) structure than in LSNO (bottom layer)/LCO (top layer), as can be inferred by comparing the resistivity curves obtained for x = 0.7. As far as lower doping levels are concerned, one expects T_c to exhibit a similar dependence on

Open Access Article. Published on 14 March 2018. Downloaded on 1/13/2026 12:12:27 PM.
This article is licensed under a Creative Commons Attribution 3.0 Unported Licence.

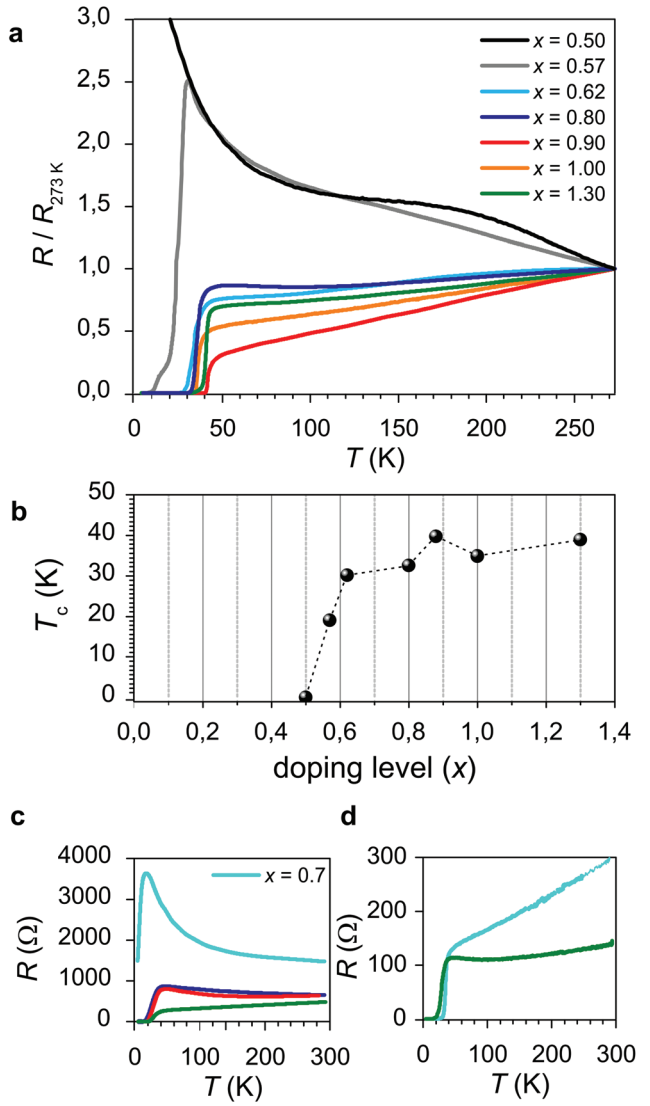

Fig. 1 Electrical properties of LCO/LSNO structures. (a) Resistance curves as a function of temperature, for a set of superlattices (N = 2.5) having different doping levels x of LSNO. In order to allow for a direct comparison between the curves, the resistance values have been normalized to R (T = 273 K). (b) Dependence of T_c on the doping level x for LCO/LSNO superlattices for a set of representative samples (the corresponding R *vs.* T curves are reported in (a)). (c) R *vs.* T for LCO (bottom layer)/LSNO (top layer) bilayers and (d) R *vs.* T for LSNO (bottom layer)/LCO (top layer) bilayers for representative doping levels x (please refer to Fig. 1a for the color legend).

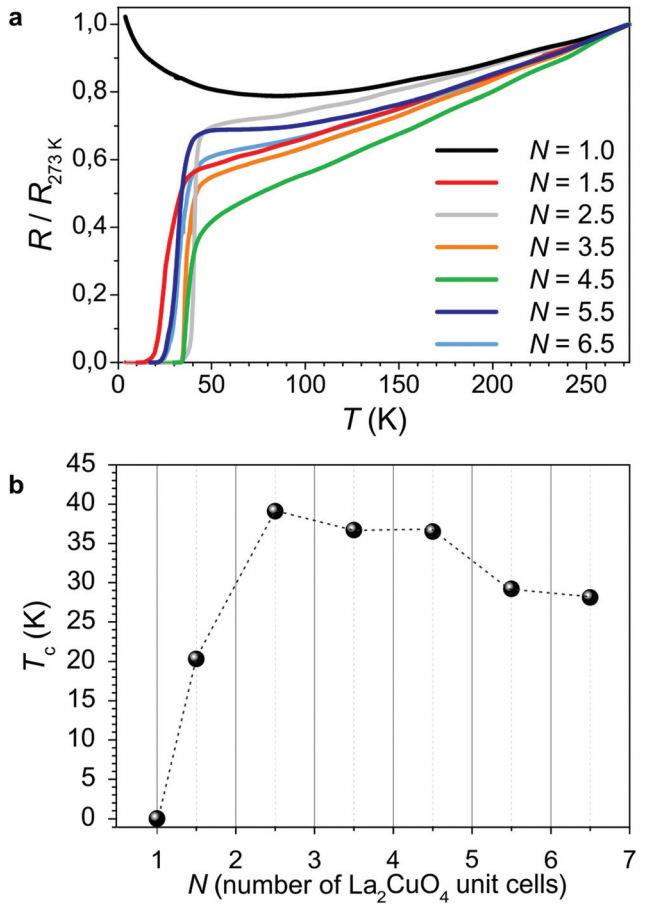

Fig. 2 Dependence of T_c on the LCO thickness for LCO/LSNO superlattices. (a) R *vs.* T curves for 1 × $La_{1.56}Sr_{0.44}CuO_4$ + S × (2.5 × $La_{0.7}Sr_{1.3}NiO_4$ + N × La_2CuO_4) superlattices, for different LCO thicknesses N. (b) T_c values as a function of the thickness N of the LCO phase for the $La_{0.7}Sr_{1.3}NiO_4/La_2CuO_4$ superlattices whose R *vs.* T curves are reported in (a).

x as was already pointed out in the case of the superlattice structures (*i.e.* absence of the superconducting transition for x < 0.5 for both the LCO/LSNO and the LSNO/LCO contacts).

The dependence of T_c on the thickness of the LCO phase has been studied for the case of superlattices in which x = 1.3 and is presented in Fig. 2. The highest T_c values (T_c > 30 K) are obtained for 2.5 u.c. < N < 4.5 u.c. For lower N values, T_c decreases (and the structure eventually becomes non-superconducting for N = 1 u.c.). For large N (>4.5 u.c.), T_c tends to saturate at ≈25 K. Notably, this is comparable to T_c obtained in the case of bilayers (*cf.* Fig. 1c and d).

In order to rationalize the findings, a systematic study has been carried out by high resolution transmission electron microscopy, employing aberration-corrected scanning transmission electron microscopy, energy-dispersive X-ray spectroscopy (EDXS) and electron energy loss spectroscopy (EELS) (Fig. 3 and 4). In particular we performed a dedicated TEM investigation on LCO/LSNO/LCO structures whose compositions (x = 0.8 and x = 0.4) determine the occurrence of remarkably different final properties: as pointed out by the electrical measurements for the bilayers (*cf.* Fig. 1c and d), the expected T_c values are ≈23–24 K at both the LCO/LSNO and the LSNO/LCO contacts for x = 0.8, whereas no superconductivity arises for x = 0.4 (irrespective of the layer sequencing).

The HAADF images (Fig. 3a and c for x = 0.8 and x = 0.4, respectively) highlight the perfect lattice match between the phases. Owing to the high Sr content in the LSNO phase (Z_{Sr} = 38, Z_{La} = 57), the LSNO layers exhibit darker contrast than LCO

 This journal is © The Royal Society of Chemistry 2018

Open Access Article. Published on 14 March 2018. Downloaded on 1/13/2026 12:12:27 PM.
This article is licensed under a Creative Commons Attribution 3.0 Unported Licence.

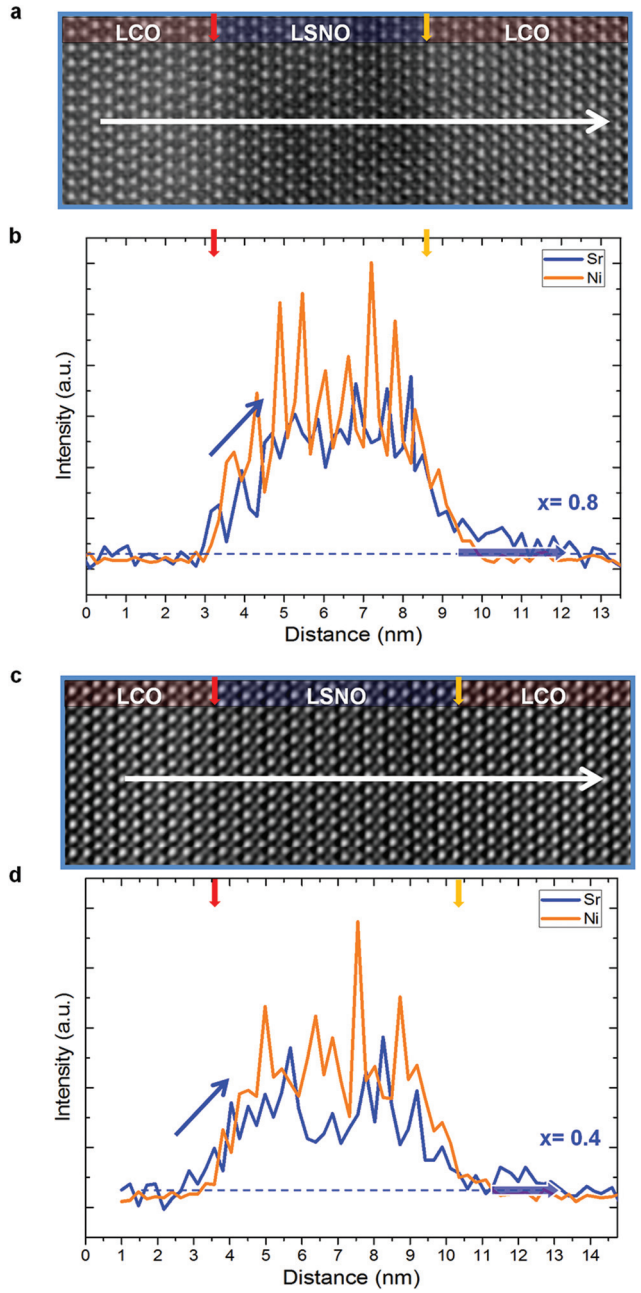

Fig. 3 TEM analysis (imaging and EDX spectroscopy) for LCO/LSNO/LCO trilayer structures. In panels (a) and (c), HAADF images of structures in which the doping level of LSNO is x = 0.8 and x = 0.4, respectively, are reported. EDX linescans for Ni and Sr are shown in panels b (for x = 0.8) and d (x = 0.4). Please note that the nominal thickness of LSNO is 4.5 u.c. for x = 0.8 and 5 u.c. for x = 0.4.

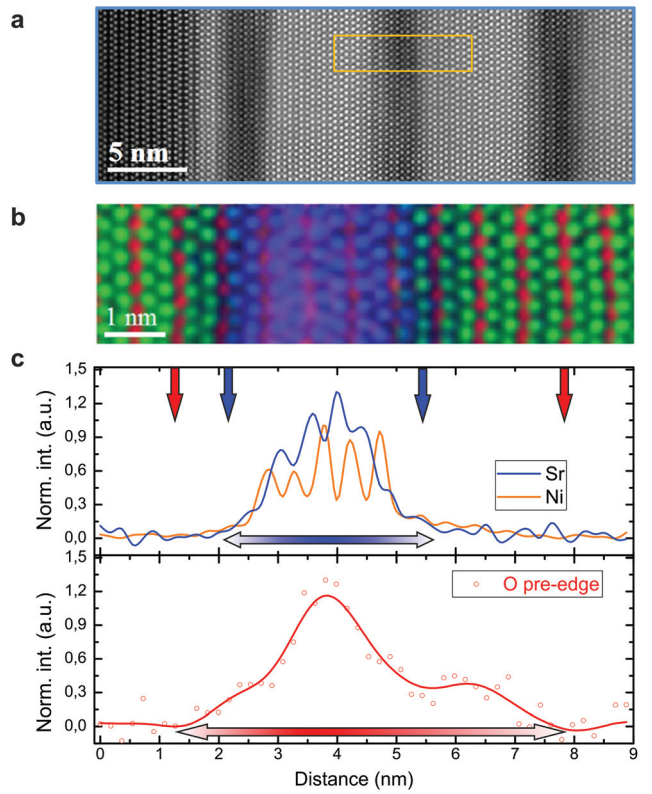

Fig. 4 HR-STEM investigation for the $La_{0.7}Sr_{1.3}NiO_4/La_2CuO_4$ interface. (a) HAADF image of a LSNO/LCO superlattice structure (N = 9). (b) Spatial elemental distribution, extracted from the EELS spectrum image across a $La_{0.7}Sr_{1.3}NiO_4$ region and neighboring LCO areas (the analyzed region is highlighted by the orange square in panel (a)). The color code is as follows: La-green, Cu-red, Ni-orange, Sr-blue. (c) EDX signal for Sr (blue) and Ni (orange) (top panel), together with the simultaneously acquired O–K edge prepeak profile as obtained by a EELS linescan (red line, bottom panel). The blue and red arrows indicate the upper limits for the Sr and holes distributions, respectively.

layers. This is particularly evident in Fig. 3a owing to the higher x content. The nominal interface positions, identified by taking into account the LSNO thickness and the number of Ni intensity maxima in the EDX linescans (*cf.* Fig. 3b for x = 0.8 and 3d for x = 0.4), are marked by a red and a yellow arrow. (Please note that the so-defined nominal interface positions are taken as a reference for the following discussion on the cat-ionic redistribution widths). There are some remarkable findings to be highlighted in relation to the effects of layer sequencing and doping level x on the chemical sharpness of the interface. Interestingly, one can observe that a certain redistribution of Ni and Sr, from the LSNO into the LCO phase, is present at both phase contacts. However, while the Sr concentration initially undergoes a sharp drop on both interface sides, whose upper limit of spread can be quantified as ≈1 nm regardless of the doping level, an additional Sr "tail", indicated by a shaded blue arrow in Fig. 3b and d, characterizes the LSNO/LCO contact only (LCO as a top layer). This is wider for x = 0.8 (≈2.6 nm) than for x = 0.4 (≈1.5 nm). Even more interesting is the comparison between the Ni and Sr profiles, in consideration of the fact that Ni impurities are known to act as a suppressor of HTSC in LCO.[41,42] In particular, the redistribution length of the two species at the LCO/LSNO contact is of the same extent. Conversely, the Sr migration width at the LSNO/LCO interface is larger than the Ni redistribution width.

In Fig. 4, we focus our attention on the comparison between the electronic and the ionic concentration profiles

Open Access Article. Published on 14 March 2018. Downloaded on 1/13/2026 12:12:27 PM.
This article is licensed under a Creative Commons Attribution 3.0 Unported Licence.

across the interface. It is well known that the analysis of the O–K edge prepeak by EELS allows one to retrieve information about the concentration of free electron holes with atomic layer precision.[43,44] First, a large area HAADF image of the superlattice structure under consideration (having x = 1.3) is reported (Fig. 4a), in which the high-quality epitaxial relationship between the substrate (dark region on the left-hand side) and the film is highlighted. In Fig. 4b and c we report the RGB EELS color map (panel b) and the hole concentration profile, together with the simultaneously acquired signals from Ni and Sr (panel c), respectively (please see ESI Fig. S4† for the experimental details). The images do not only show that, similarly to what is described above, a certain cationic intermixing at the phase contacts is present, but also that, most interestingly, a decoupling between the Sr and the hole concentrations can be noticed, as highlighted by the different widths between the Sr profile (blue line in Fig. 4c, top panel) and the O–K edge prepeak (red line in Fig. 4c, bottom panel). This is present at both interface sides, *i.e.* at the LCO/LSNO interface and at the LSNO/LCO contact.

3. Discussion

According to the detailed TEM investigations which are presented in Fig. 3 and 4, cationic redistribution occurs at the interfaces. Even though it is very limited, a role in the occurrence of HTSC can be attributed to the unintentional Sr doping of LCO. Cationic intermixing at epitaxial interfaces has been reported several times in the literature and represents one of the key aspects in this type of system since it may deeply affect, or even be mainly responsible for the peculiar functionalities of epitaxial interfaces. As a matter of fact, certain intermixing is often observed, but its width and its effect on the system properties (being arguably dependent on the deposition process) are in many cases still under debate.[31,45–47] Our case is particularly interesting since it exhibits an asymmetric behavior for the two interfaces, whose intermixing width depends on the layer sequence. Such a finding has been highlighted in the case of epitaxial semiconducting structures (*cf. e.g.* ref. 48) and only in few cases in the context of oxide systems (*e.g.* $LaVO_3/SrTiO_3$, $LaMnO_3/SrMnO_3$ and two-dimensionally Sr-doped LCO).[49–51] Such an asymmetric profile may be arguably ascribed to the combined effect of thermal diffusion acting on both interface sides (see ESI Fig. S3†) and a "Muraki segregation effect",[52] the latter acting in the growth direction only (*i.e.* at the LSNO/LCO contact), in analogy with a previous study on a related system.[51]

However, Sr intermixing alone does not provide a sufficient explanation for a number of experimental findings and therefore, it cannot be accounted as the only phenomena responsible for interface HTSC, as we detail in the following points. (i) While, as far the LSNO/LCO contact is concerned, we observe a greater Sr redistribution width for the superconducting interface (when x = 0.8) with respect to a non-superconducting contact (x = 0.4), no difference in the chemical abruptness at the LCO/LSNO interface (LCO as a bottom layer) can be detected when comparing the situation in which x = 0.8 (superconducting interface – Fig. 3b) with the one in which x = 0.4 (non-superconduting interface – Fig. 3d). Therefore, the electrical properties are not directly coupled to the Sr concentration profiles. (ii) The LCO/LSNO interface is not only chemically sharper in terms of Sr, but it is also characterized by a similar distribution width of Sr and Ni, *i.e.* Ni impurities are present in the same LCO region which is also doped by Sr. As it is well known in the literature and further corroborated by our experimental evidence (ESI Fig. S5†), the presence of a small percentage of Ni replacing Cu in the CuO_2 planes is expected to determine a strong decrease of the superconducting critical temperature, T_c.[41,42] Therefore, if cationic interdiffusion is taken as the only culprit for the effects, superconductivity with a T_c up to 40 K stemming from such a Ni-containing LSCO region would have to be ruled out. (iii) Lastly, the comparison between the Sr dopant and the hole concentration profiles, as retrieved by TEM spectroscopy (Fig. 4c), indicates that an evident decoupling between the two carriers occurs in the form of a hole accumulation layer at the interface. Such a finding is clearly not ascribable to "simple" homogeneous doping, in which charge neutrality is locally fulfilled according to eqn (1) (which can be simplified as $p = [Sr'_{La}]$ in the hole compensation regime).

At this point, it is important to note that, as in these systems, both the ionic (cationic and anionic) and the electronic species are sufficiently mobile to redistribute,[35] a generalized thermodynamic picture that takes into account all these constituting elements has to be paid attention to.[38] In particular at the interface, in order to describe the thermodynamic equilibrium in the system, one needs to consider the electrochemical potential $\tilde{\mu}_k$ for each defect species k having effective charge z_k:

$$\begin{aligned}\tilde{\mu}_k(x) &= \mu_k + z_k e\varphi(x) \\ &= \mu_k^0 + RT\log c_k(x) + z_k e\varphi(x)\end{aligned} \tag{3}$$

in which the electrochemical potential at distance x from the interface is expressed as a function of the standard chemical potential μ_k^0, of the defect concentration c_k and of the electrical potential $\varphi(x)$ (here μ_k represents the chemical potential for the defect k). In eqn (3), we assumed for simplicity dilute carrier concentration and hence Boltzmann distribution.

In equilibrium, the condition of constant electrochemical potential demands

$$\tilde{\mu}_k(x) = \tilde{\mu}_{k,\infty}, \tag{4}$$

$\tilde{\mu}_{k,\infty} = \tilde{\mu}_k$ ($x = \infty$) being the electrochemical potential in the bulk ($x = \infty$).

The chemical potential gradient for the defect species (holes, oxygen vacancies, and Sr), which is present at the interface between LSNO and LCO, is not only a driving force for the migration of Sr in the direction of LCO (as described above), but also for the transfer of holes and oxygen vacancies. Owing to the mobilities involved, the latter is expected to occur even

 This journal is © The Royal Society of Chemistry 2018

Open Access Article. Published on 14 March 2018. Downloaded on 1/13/2026 12:12:27 PM.
This article is licensed under a Creative Commons Attribution 3.0 Unported Licence.

at room temperature, while a Sr-transfer requires higher temperatures (possibly reached during preparation). As far as the charge transfer direction is concerned, the entire free energy picture has to be considered. Here we estimate – supported by the chemical similarity of the base-materials – the direction on the basis of the doping conditions (configurational entropy). As the substantial Sr-doping of LNO enforces a very high hole and a very high vacancy concentration as long as electroneutrality has to be fulfilled, suspending the latter condition is expected to result in transfer of both carriers to the undoped LCO provided Sr remains frozen (or also to a Sr-redistribution if sufficiently mobile). For Boltzmann distribution, the equilibrium spatial distribution in such a space-charge region follows from combining eqn (3) and (4):

$$\frac{c_k(x)}{c_{k,\infty}} = \exp\left(-\frac{z_k e \Delta\varphi(x)}{kT}\right) \quad (5)$$

$c_{k,\infty}$ being the defect concentration in the bulk and $\Delta\varphi(x) = \varphi(x) - \varphi(x = \infty)$ the space-charge potential.

Eqn (5) shows that *e.g.* oxygen vacancies and holes perceive the space-charge in a qualitatively similar way, but the profile for $V_O^{\bullet\bullet}$ ($z_k = 2$) is steeper than for $h^\bullet$ ($z_k = 1$). A net transfer of oxygen vacancies and holes from LSNO to LCO leads to the formation of a negatively charged region at the LSNO side of the interface. For compensation, a region where oxygen vacancies and especially holes (the holes being the majority defect in the system) are accumulated, establishes in LCO. Such a situation with an enriched p-type charge carrier concentration eventually leads to the occurrence of HTSC in LCO at the interface.

A schematic picture of the thermodynamic situation at the interface is depicted in Fig. 5.

Such a space-charge situation is able to explain all the experimental findings. (i) From the experimental data, it is evident that the key element for the appearance of superconductivity is the enhanced hole concentration in LSNO. This suggests electron transfer (electronic space-charge): in order to maintain the hole electrochemical potential constant (see eqn (4)), holes are transferred from LSNO into the LCO phase leading to the appearance of HTSC.[39] Such a mechanism has already found experimental proof in other oxides.[14,53] Interestingly, for high doping level ($x \geq 0.9$), single phase LSNO undergoes an insulator-to-metal transition as reported in the literature and as confirmed by our previous studies on MBE-grown LSNO films:[32,40] Such a value is very similar to the doping level at which the superconducting state is fully developed in the structure studied here, therefore suggesting that charge transfer mainly involves delocalized holes from the metallic LSNO phase to LCO. It should be noted that this is also in line with previous contributions on a related system (*i.e.* interface HTSC in LSCO/LCO bilayers),[54] in which a similar dependence of T_c on the electronic carrier density of LSCO was found. (ii) Hole-Sr decoupling (*cf.* Fig. 3d) can be fully explained by considering that, in the space-charge regions, the concentration profiles of the mobile defects are not dictated by the condition of local electroneutrality (*cf.* eqn (1) and (5)). Rather, the migration of negatively charged Sr defects from LSNO to LCO is expected to simply lower the space-charge potential $\varphi(x)$. (iii) As far as the effect of Ni impurities on HTSC is concerned, it is evident from Fig. 3d that the extent of the hole accumulation (space-charge) zone at the interface, in which HTSC is expected to appear, is larger than the Ni redistribution width. (iv) Lastly, the dependence of T_c on the superlattice spacing N (Fig. 2) can be explained by taking into account that for low spacing (for which a reduced T_c was found) one expects the space-charge zones to overlap, leading to a high hole concentration (overdoping regime of superconductivity). The reduced T_c (≈25 K) which has been observed for very large spacing ($N > 5$), as well as for the bilayers (Fig. 1c and d), may instead be ascribed to out-of-plane adjustments of the lattice bond lengths as a consequence of the epitaxial relation between the layers.[39,55] It is noteworthy that very few recent studies have dealt with the origin of the electrical and magnetic properties of oxide epitaxial heterostructures in the light of the space-charge theory.[56,57] Moreover, we recently investigated the modulation of the charge carrier concentration in two-dimensionally doped superconducting lanthanum cuprate (La_2CuO_4).[19] It was shown that such an effect stems, at the side of the interface facing the substrate, from a hole accumulation layer, which is a consequence of local space-charge effects.

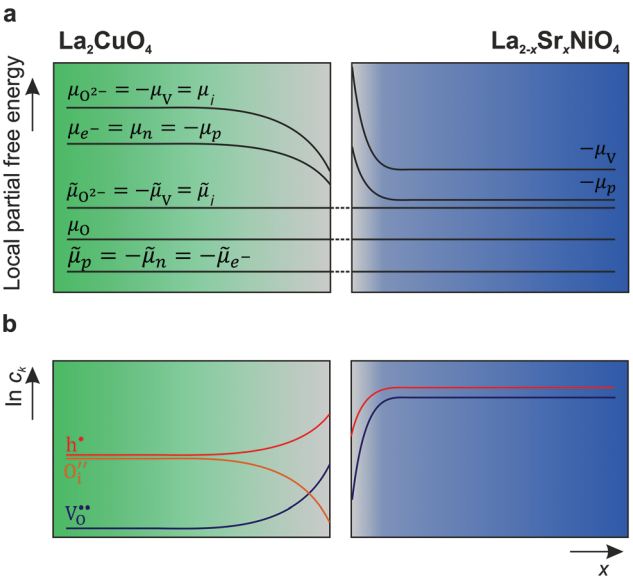

Fig. 5 Sketch of the thermodynamic situation at the boundary layers of LCO and LSNO (if both are equilibrated with the same oxygen partial pressure and a net transfer of holes and vacancies occurs from LSNO to LCO). (a) The condition of thermodynamic equilibrium for the defect species (the abbreviations *v, i, p, n* are used for the building units oxygen vacancies, oxygen interstitials, electrons and holes respectively) and with the external oxygen partial pressure defines a horizontal profile for the electrochemical potential of $V(\tilde{\mu}_V = \mu_V + 2F\varphi)$ and $p(\tilde{\mu}_p = \mu_p + F\varphi)$, as well as for the chemical potential of oxygen $\mu_O = -\mu_V + 2\mu_p$. Therefore, as a consequence of the difference in the bulk chemical potentials for the defect species, the bending of μ_V and μ_p at the interface is expected. (b) Resulting charge concentration profiles at the interface.

Open Access Article. Published on 14 March 2018. Downloaded on 1/13/2026 12:12:27 PM.
This article is licensed under a Creative Commons Attribution 3.0 Unported Licence.

It should be repeated that, according to the condition of electrochemical potential constancy, also $V_O^{\cdot\cdot}$ values (which are abundant in LSNO due to the high doping level)[37,58] are expected to rearrange at the interface together with holes. A redistribution of both according to eqn (5) automatically fulfills the condition of constant chemical potential of neutral oxygen at the interfaces, provided that both materials are in equilibrium with the same oxygen partial pressure (Fig. 5). Notably, we expect a stronger interface electrical potential and consequently a greater hole accumulation if both $V_O^{\cdot\cdot}$ and $h^{\cdot}$ redistribute, while a partial Sr-redistribution would lower the space-charge effect. According to Fig. 4, the estimated hole decay length for LCO is ≈1–2 nm. It should be noted that the expected steeper concentration profile of $V_O^{\cdot\cdot}$ with respect to $h^{\cdot}$ (*cf.* eqn (5)) may affect the final properties of the LCO region which is adjacent to the interface, leading to overdoping.[59] Although the limited resolution of the methods employed in the present studies (HR-STEM) for anions did not allow for the direct quantification of the $V_O^{\cdot\cdot}$ across the interface, it is worth mentioning that the formation of a space-charge zone due to ionic transfer has already been reported in the literature in systems such as BaF_2/CaF_2 or LiF/TiO_2.[9,60,61] As far as oxygen defects are concerned, it was only demonstrated for grain boundaries.[6,10,62–64]

Lastly, one should also consider that a certain role in the definition of the interface functionalities could be played by nonidealities stemming *e.g.* from interface roughness (terraces), which may aggravate the formation of a percolative HTSC path. In the case of pronounced roughness, such pathways rely on interconnected LSCO nano-islands, laterally separated by LSNO (nanoscale phase separation). Such a scenario would explain the appearance of HTSC at the interface even in the presence of Ni and the suppressed diamagnetic response of the superconducting phase, as measured by using the mutual inductance set-up, arguably due to the partial lack of percolation of the superconducting layer (see ESI Fig. S6†).[65] On the other hand, no direct evidence of such a situation could be retrieved from TEM analysis, which instead highlights the presence of a hole accumulation layer at the interface. The latter can only be explained if a space-charge scenario is taken into account, therefore nanoscale phase-separation alone cannot be considered as a final explanation.

4. Conclusion

In conclusion, we presented a study on the structural and electrical properties of lanthanum cuprate/Sr-doped lanthanum nickelate epitaxial heterostructures, grown by the atomic-layer-by-layer method *via* oxide molecular beam epitaxy. The structures exhibit high-temperature superconductivity (T_c up to ≈40 K) as a consequence of local hole accumulation and we showed that T_c can be tuned by changing the doping level x in the nickelate or by varying the supercell thickness. In particular, HTSC occurs only when a highly doped (metallic) LSNO composition is employed. Structural analysis by HR-STEM showed that a certain cationic interdiffusion (≈1 u.c.), involving both the A-site (La, Sr) and the B-site cations, is present. A certain tendency for Sr to migrate further from LSNO into LCO in the growth direction was detected, while the LCO/LSNO interface is chemically sharper. Moreover, EELS investigations suggest the presence of a hole accumulation layer at the interface, which is decoupled from the ionic dopant profile. Simple cationic interdiffusion does not satisfactorily explain all the experimental findings; rather, the system can be fully described if a mechanism for which space-charge effects (*i.e.* migration of holes and oxygen vacancies from the LSNO into the LCO phase) are taken into account. Our findings not only represent an unprecedented case of interface high-temperature superconductivity in the case of heteroepitaxy, but may also shed light on the complex interplay between ionic and electronic effects at oxide interfaces, and in particular on typically neglected effects of oxygen vacancy redistribution.

5. Experimental section

Film heterostructures of La_2CuO_4 and $La_{2-x}Sr_xNiO_4$ were deposited on $LaSrAlO_4$ (001) substrates (Crystec GmgH and Crystal GmbH) by ozone-assisted molecular beam epitaxy (DCA Instruments) using the atomic-layer-by-layer method. Typical deposition conditions are T = 600 °C, $p = 2 \times 10^{-5}$ mTorr. A more detailed description of the deposition method can be found in ref. 27. All the samples were *in situ* vacuum annealed after the growth (T = 200 °C) for ensuring no contribution to electrical conductivity by oxygen interstitial doping (see eqn (1) and ref. 40). A thin buffer layer (1 u.c. metallic $La_{1.56}Sr_{0.44}CuO_4$) was routinely deposited on the substrate in order to improve the film/substrate interface, thus promoting the conditions for epitaxial growth. Electrical conductivity measurements were performed in Van Der Pauw geometry employing Pt electrodes, during heating cycles from liquid He temperature, by using a motorized dipstick with an automated control loop (heating rate <0.05 K s^{-1}). Film diamagnetic response was measured in transmission geometry by using Cu coils. The typical drive current was 60 μA, 1.6 kHz. The setup was equipped with a SR850DSP lock-in amplifier and Agilent 34401A multimeters.

TEM specimens for the investigations were thinned to electron transparency by tripod polishing (≤10 μm), which is followed by argon ion beam milling in a stage cooled with liquid nitrogen. The electron microscopy and spectroscopy experiments were performed on a probe C_s corrected JEOL ARM 200CF microscope equipped with a cold field-emission electron source, a large solid-angle SDD-type JEOL Centurio EDX detector and a Gatan GIF Quantum ERS spectrometer. The microscope was operated at 200 kV, a semi-convergence angle (a) of 21 mrad, giving rise to a probe size of 0.8 Å (1 Å for the analytical analysis). A collection semi-angle (b) of 68.5 mrad was used for EELS analyses and the collection angle (109–270 mrad) was used for HAADF images. Please note the EDXS measurements were performed at a thickness less than

 This journal is © The Royal Society of Chemistry 2018

Open Access Article. Published on 14 March 2018. Downloaded on 1/13/2026 12:12:27 PM.
This article is licensed under a Creative Commons Attribution 3.0 Unported Licence.

30 nm (t/λ < 0.4 confirmed by EELS low loss measurement), where the beam broadening is the lowest, thus the signal delocalization while we discuss the cationic intermixing can be ruled out.[66]

Conflicts of interest

There are no conflicts to declare.

Acknowledgements

We thank U. Salzberger for TEM specimen preparation, P. Specht and B. Stuhlhofer for the technical support on the Oxide MBE system, and B. Stuhlhofer, Y. Stuhlhofer and S. Schmid for contact deposition. I. Garbayo is thanked for critically reading the manuscript. Y. E. S, Y. W., W. S. and P. A. v. A acknowledge funding from the European Union Seventh Framework Program (FP7/2007-2013) under grant agreement no. 31248. Open Access funding provided by the Max Planck Society.

References

1 J. Mannhart and D. G. Schlom, *Science*, 2010, **327**, 1607–1611.
2 J. Maier, *J. Electrochem. Soc.*, 1987, **134**, 1524–1535.
3 A. Tschöpe, *Solid State Ionics*, 2001, **139**, 267–280.
4 C. C. Chen, L. Fu and J. Maier, *Nature*, 2016, **536**, 159–164.
5 G. Hammerl, a Schmehl, R. Schulz, B. Goetz, H. Bielefeldt, C. Schneider, H. Hilgenkamp and J. Mannhart, *Nature*, 2000, **407**, 162–164.
6 P. Lupetin, G. Gregori and J. Maier, *Angew. Chem., Int. Ed.*, 2010, **49**, 10123–10126.
7 K. K. Adepalli, M. Kelsch, R. Merkle and J. Maier, *Adv. Funct. Mater.*, 2013, **23**, 1798–1806.
8 E. Navickas, Y. Chen, Q. Lu, W. Wallisch, T. M. Huber, J. Bernardi, M. Stöger-Pollach, G. Friedbacher, H. Hutter, B. Yildiz and J. Fleig, *ACS Nano*, 2017, **11**, 11475–11487.
9 J. Maier, *Prog. Solid State Chem.*, 1995, **23**, 171–263.
10 G. Gregori, R. Merkle and J. Maier, *Prog. Mater. Sci.*, 2017, **89**, 252–305.
11 A. Ohtomo and H. Y. Hwang, *Nature*, 2004, **427**, 423–426.
12 C. Cen, S. Thiel, J. Mannhart and J. Levy, *Science*, 2009, **323**, 1026–1030.
13 K. S. Takahashi, M. Kawasaki and Y. Tokura, *Appl. Phys. Lett.*, 2001, **79**, 1324–1326.
14 A. Brinkman, M. Huijben, M. van Zalk, J. Huijben, U. Zeitler, J. C. Maan, W. G. van der Wiel, G. Rijnders, D. H. a Blank and H. Hilgenkamp, *Nat. Mater.*, 2007, **6**, 493–496.
15 J. M. N. Reyren, S. Thiel, D. A. Muller and J.-M. Triscone, *Science*, 2007, **317**, 1196.
16 J. Biscaras, N. Bergeal, A. Kushwaha, T. Wolf, A. Rastogi, R. C. Budhani and J. Lesueur, *Nat. Commun.*, 2010, **1**, 89.
17 A. Gozar, G. Logvenov, L. F. Kourkoutis, a. T. Bollinger, L. a. Giannuzzi, D. A. Muller and I. Bozovic, *Nature*, 2008, **455**, 782–785.
18 D. Di Castro, M. Salvato, A. Tebano, D. Innocenti, C. Aruta, W. Prellier, O. I. Lebedev, I. Ottaviani, N. B. Brookes, M. Minola, M. Moretti Sala, C. Mazzoli, P. G. Medaglia, G. Ghiringhelli, L. Braicovich, M. Cirillo and G. Balestrino, *Phys. Rev. B: Condens. Matter Mater. Phys.*, 2012, **86**, 1–7.
19 F. Baiutti, G. Logvenov, G. Gregori, G. Cristiani, Y. Wang, W. Sigle, P. A. van Aken and J. Maier, *Nat. Commun.*, 2015, **6**, 1–8.
20 C. Aruta, G. Ghiringhelli, V. Bisogni, L. Braicovich, N. B. Brookes, A. Tebano and G. Balestrino, *Phys. Rev. B: Condens. Matter Mater. Phys.*, 2009, **80**, 1–8.
21 C. W. Bark, D. A. Felker, Y. Wang, Y. Zhang, H. W. Jang, C. M. Folkman, J. W. Park, S. H. Baek, H. Zhou, D. D. Fong, X. Q. Pan, E. Y. Tsymbal, M. S. Rzchowski and C. B. Eom, *Proc. Natl. Acad. Sci. U. S. A.*, 2011, **108**, 4720–4724.
22 S. Okamoto and A. J. Millis, *Nature*, 2004, **428**, 630–633.
23 Y. Z. Chen, N. Bovet, F. Trier, D. V. Chrsitensen, F. M. Qu, N. H. Andersen, T. Kasama, W. Zhang, R. Giraud, J. Dufouleur, T. S. Jespersen, J. R. Sun, A. Smith, J. Nygård, L. Lu, B. Buechner, B. G. Shen, S. Linderoth and N. Pryds, *Nat. Commun.*, 2013, **4**, 1371.
24 C. Lin and A. A. Demkov, *Phys. Rev. Lett.*, 2014, **113**, 1–5.
25 B. W. Veal, S. K. Kim, P. Zapol, H. Iddir, P. M. Baldo and J. A. Eastman, *Nat. Commun.*, 2016, **7**, 11892.
26 M. Gibert, M. Viret, A. Torres-Pardo, C. Piamonteze, P. Zubko, N. Jaouen, J. M. Tonnerre, A. Mougin, J. Fowlie, S. Catalano, A. Gloter, O. Stéphan and J. M. Triscone, *Nano Lett.*, 2015, **15**, 7355–7361.
27 F. Baiutti, F. Wrobel, G. Christiani and G. Logvenov, in *Metal Oxide-based Thin Film Structures: Formation, Characterization and Application of Interface-based Phenomena*, Elsevier, 2018, pp. 53–78.
28 P. G. Radaelli, D. G. Hinks, A. W. Mitchell, B. A. Hunter, J. L. Wagner, B. Dabrowski, K. G. Vandervoort, H. K. Viswanathan and J. D. Jorgensen, *Phys. Rev. B: Condens. Matter Mater. Phys.*, 1994, **49**, 4163–4175.
29 H. Sato, M. Naito and H. Yamamoto, *Phys. C*, 1997, **280**, 178–186.
30 S. Smadici, J. C. T. Lee, S. Wang, P. Abbamonte, G. Logvenov, A. Gozar, C. D. Cavellin and I. Bozovic, *Phys. Rev. Lett.*, 2009, **102**, 1–4.
31 Y. E. Suyolcu, Y. Wang, F. Baiutti, A. Al-Temimy, G. Gregori, G. Cristiani, W. Sigle, J. Maier, P. A. Van Aken and G. Logvenov, *Sci. Rep.*, 2017, **7**, 453.
32 S. Shinomori, Y. Okimoto, M. Kawasaki and Y. Tokura, *J. Phys. Soc. Jpn.*, 2002, **71**, 705–708.
33 H. Sato, A. Tsukada, M. Naito and A. Matsuda, *Phys. Rev. B: Condens. Matter Mater. Phys.*, 2000, **61**, 12447–12456.
34 J. Maier and G. Pfundtner, *Adv. Mater.*, 1991, **3**, 292–297.
35 E. Opila, H. Tuller, B. J. Wuensch and J. Maier, *J. Am. Ceram. Soc.*, 1993, **76**, 2363–2369.
36 D. E. Rice and D. J. Buttrey, *J. Solid State Chem.*, 1993, **105**, 197–210.

Open Access Article. Published on 14 March 2018. Downloaded on 1/13/2026 12:12:27 PM.
This article is licensed under a Creative Commons Attribution 3.0 Unported Licence.

37 J. P. Tang, R. I. Dass and A. Manthiram, *Mater. Res. Bull.*, 2000, **35**, 411–424.
38 J. Maier, *J. Phys. Chem. Solids*, 1985, **46**, 309–320.
39 F. Baiutti, *Heterogeneous doping and superconductivity in La_2CuO_4-based heterostructures*, University of Stuttgart, 2015.
40 F. Baiutti, G. Christiani and G. Logvenov, *Beilstein J. Nanotechnol.*, 2014, **5**, 596–602.
41 G. D. Liu, Z. X. Zhao and G. C. Che, *Solid State Commun.*, 1999, **109**, 495–499.
42 M. Matsuura, M. Fujita, H. Hiraka, M. Kofu, H. Kimura, S. Wakimoto, T. G. Perring, C. D. Frost and K. Yamada, *Phys. Rev. B*, 2012, **134529**, 1–8.
43 H. Romberg, M. Alexander, N. Ñcker, P. Adelmann and J. Fink, *Phys. Rev. B: Condens. Matter Mater. Phys.*, 1990, **42**, 8768–8771.
44 Y. Wang, F. Baiutti, G. Gregori, G. Cristiani, U. Salzberger, G. Logvenov, J. Maier and P. A. Van Aken, *ACS Appl. Mater. Interfaces*, 2016, **8**, 6763–6769.
45 M. Luysberg, M. Heidelmann, L. Houben, M. Boese, T. Heeg, J. Schubert and M. Roeckerath, *Acta Mater.*, 2009, **57**, 3192–3198.
46 G. Salvinelli, G. Drera, A. Giampietri and L. Sangaletti, *ACS Appl. Mater. Interfaces*, 2015, **7**, 25648–25657.
47 Y. E. Suyolcu, Y. Wang, W. Sigle, F. Baiutti, G. Cristiani, G. Logvenov, J. Maier and P. A. van Aken, *Adv. Mater. Interfaces*, 2017, **4**, 24.
48 E. F. Schubert, *J. Vac. Sci. Technol., A*, 1990, **8**, 2980.
49 L. F. Kourkoutis, D. a Muller, Y. Hotta and H. Y. Hwang, *Appl. Phys. Lett.*, 2007, **91**, 163101.
50 S. J. May, A. B. Shah, S. G. E. Te Velthuis, M. R. Fitzsimmons, J. M. Zuo, X. Zhai, J. N. Eckstein, S. D. Bader and A. Bhattacharya, *Phys. Rev. B: Condens. Matter Mater. Phys.*, 2008, **77**, 2–6.
51 F. Baiutti, G. Gregori, Y. Wang, Y. E. Suyolcu, G. Cristiani, P. A. Van Aken, J. Maier and G. Logvenov, *ACS Appl. Mater. Interfaces*, 2016, **8**, 27368–27375.
52 K. Muraki, S. Fukatsu, Y. Shiraki and R. Ito, *Appl. Phys. Lett.*, 1992, **61**, 557–559.
53 A. Ohtomo, D. A. Muller, J. L. Grazul and H. Y. Hwang, *Nature*, 2002, **419**, 378–380.
54 J. Wu, O. Pelleg, G. Logvenov, a T. Bollinger, Y.-J. Sun, G. S. Boebinger, M. Vanević, Z. Radović and I. Božović, *Nat. Mater.*, 2013, **12**, 877–881.
55 V. Y. Butko, G. Logvenov, N. Božović, Z. Radović and I. Božović, *Adv. Mater.*, 2009, **21**, 3644–3648.
56 F. Gunkel, R. Waser, A. H. H. Ramadan, R. A. De Souza, S. Hoffmann-Eifert and R. Dittmann, *Phys. Rev. B*, 2016, **93**, 245431.
57 F. Gunkel, C. Bell, H. Inoue, B. Kim, A. G. Swartz, T. A. Merz, Y. Hikita, S. Harashima, H. K. Sato, M. Minohara, S. Hoffmann-Eifert, R. Dittmann and H. Y. Hwang, *Phys. Rev. X*, 2016, **6**, 31035.
58 V. V. Vashook, I. I. Yushkevich, L. V. Kokhanovsky, L. V. Makhnach, S. P. Tolochko, I. F. Kononyuk, H. Ullmann and H. Altenburg, *Solid State Ionics*, 1999, **119**, 23–30.
59 G. Kim, G. Christiani, G. Logvenov, S. Choi, H.-H. Kim, M. Minola and B. Keimer, *Phys. Rev. Mater.*, 2017, **1**, 54801.
60 N. Sata, K. Eberman, K. Eberl and J. Maier, *Nature*, 2000, **408**, 946–949.
61 C. Li, L. Gu, X. Guo, D. Samuelis, K. Tang and J. Maier, *Nano Lett.*, 2012, **12**, 1241–1246.
62 X. Guo, J. Fleig and J. Maier, *J. Electrochem. Soc.*, 2001, **148**, J50.
63 M. Vollman and R. Waser, *J. Am. Ceram. Soc.*, 1994, **77**, 235–243.
64 I. Denk, J. Claus and J. Maier, *J. Electrochem. Soc.*, 1997, **144**, 3526–3536.
65 X. He, A. Gozar, R. Sundling and I. Božović, *Rev. Sci. Instrum.*, 2016, **87**, 113903.
66 S. R. Spurgeon, Y. Du and S. A. Chambers, *Microsc. Microanal.*, 2017, **23**, 513–517.

This journal is © The Royal Society of Chemistry 2018